ISSN: 2640-5571

Research Article

Advances in Nanoscience and Nanotechnology

Loading of Sn Nanoparticle-Decorated Silymarin on to Graphene Oxide for Effective Inhibition of Cancer Cell Viability

Hossein Abbasinia[1]*, Hanieh Sadeghi[2] and Naba Najar[3]

[1]*Department of Cellular and Molecular Biology, Faculty of Advanced Sciences and Technology, Tehran Medical Sciences, Islamic Azad University, 1949635881, Tehran, Iran.*

[2]*Department of Stem Cells and Developmental Biology, Cell Science Research Center, Roan institute for Stem Cell Biology and Technology, ACECR, 1648745854, Tehran, Iran.*

[3]*Department of Biochemistry, Faculty of medicine, Iran University of Medical Sciences, Tehran, Iran.*

***Corresponding Author**

Hossein Abbasinia, Department of Cellular and Molecular Biology, Faculty of Advanced Sciences and Technology, Tehran Medical Sciences, Islamic Azad University, 1949635881, Tehran, Iran.

Submitted: 2023, Nov 20; **Accepted:** 2023, Dec 12; **Published:** 2023, Dec 27

Citation: Abbasinia, H., Sadeghi, H., Najar, N., (2023).loading of Sn nanoparticle-decorated Silymarin on to grapheme oxide for effective inhibition of cancer cell viability. *Adv Nanoscie Nanotec, 7*(1), 72-80.

Abstract

The aim of this study was to synthesize a novel Nan composite (GO/SM/Sn Nan composite) consist of silymarin (SM) loaded (CH3)2SnCl2 based on grapheme oxide (GO) in order to enhance cytotoxicity of SM. GO/SM/Sn Nano composite was synthesized based on general methods. The GO/SM/Sn Nano composite was characterized by TEM, FE-SEM, FTIR, XRD and DLS techniques. Cells were treated at the range of concentrations of SM and GO/SM/Sn Nano composite and cell viability was examined through MTT assay. Apoptosis rate, intracellular ROS level and cell cycle arrest were determined using specific assays and flow cytometrytechnique. Apoptotic gene expression was also analyzed by the application of real-time PCR system. GO/SM/Sn Nano composite could effectively increase inhibitory effect of SM on cancer cell viability. We found that SW480 and MCF-7 cell treatment with GO/SM/Sn leads to increased intracellular ROS level and apoptosis. It was also revealed that GO/SM/Sn could change BAX and BCL2 gene expression profile to induce apoptosis. Moreover, GO/SM/Sn caused cell cycle arrest in MCF-7 cells, which was more significant than those observed in SW480 cells. Our conclusion is that silymarin immobilization can serve as an effective method to impede the adverse side effects of other conventional treatment strategies and as a novel composite enhance the efficiency of SM administration.

Keywords: Cancer, SW480 cell line, MCF-7 Cell Line, Silymarin, Cell viability.

1. Introduction

Cancer is a multifaceted disease that arises as the consequence of deregulated growth of malignant cells that can invade and spread throughout the body. Cancer mortality has an ever-increasing rate every year and poses a huge challenge to human health around the world. In spite of attempts to find effective treatments over the past decade, there are still no curative options to manage malignant diseases including cancer. Current strategies such as chemotherapy, radiotherapy and the combination of both treatments are the most common approaches toward cancer eradication. However, due to non-specific function of these agents, their adverse side effects are undeniable. Chemotherapeutic and radio-therapeutic agents can damage healthy normal cells and tissues and induce drug resistance. Thus, there is a crucial need to find novel, efficient and selective treatment approaches for cancer treatment. Emerging evidences obtained from cell-based studies and animal model systems have revealed that natural products have both chemo preventive and chemotherapeutic effects. These compounds belong to several structural classes including alkaloids, terpenoids, polyphenols and organ sulfur compounds. Silymarin (SM) is a combination of flavonoids and flavonolignans, which is extracted from milk thistle. It has been shown that SM exhibits several therapeutic effects including anti-inflammatory, anti-carcinogenic, antioxidant and proapoptotic properties. However, low aqueous solubility and intestinal absorption of SM leads to its limited bioavailability and administration. Immobilization has attracted a great deal of attention to overcome low water solubility and limited bioavailability of hydrophobic compounds such as SM. Intriguingly, encapsulated nanoparticles are capable of controlling the bioactive compound release in the intended site. Based on this information, we hypothesized that immobilization of silymarin would be an effective option to decrease cancer cell growth and viability. Therefore, in this study, we aimed to

investigate the effect of the new GO/SM/Sn Nan composite on the viability of SW480 and MCF-7 cancer cell lines [1-14].

2. Experimental

2. 1 GO/SM/Sn Synthesis

Grapheme oxide was purchased from Daypetronic (Tehran, Iran). SM and (CH3)2SnCl2 salt were obtained from Sigma Aldrich (USA). In order to synthesize the GO/SM/Sn structure, we prepared a solution of 100 mg GO in 100 ml ethanol 96 % and incubated the solution in ultrasonic homogenizer at 30 ℃ for 30 min, followed by a second incubation at 70 ℃ for 15 min. SM solution was prepared by dissolving 100 mg SM in 25 ml ethanol 96 % and incubating in the ultrasonic homogenizer at 20 ℃ for 10 min. Then the SM solution was dropped down to the heated GO solution at 100 ℃. In the next step, the ethologic solution of (CH3)2SnCl2 (2.25 mg/ml) was added to the SM-GO mixture and refluxed for 60 min to ensure complete dissolution of (CH3)2SnCl2. Finally, the mixture was filtered and dried at 90℃ in an oven.

2. 2 Characterization of the GO/SM/Sn Structure

To determine the size and morphology of the synthesized Nano composite, transmission electron microscopy (TEM) (Zeiss-EM10C-100 KV; Carl Zeiss Mediate AG, Jena, Germany) and scanning electron microscopy (SEM) (FEI ESEM QUANTA 200, USA) were applied. To determine surface morphology of the Nano composite and confirm the participating elements in the Nano composite structure, field emission scanning electron microscopy (FE-SEM) was applied.

X-ray diffract meter (PW1730, voltage: 40 kV, current: 30 mA; Philips, Amsterdam, the Netherlands) was used to analyze crystal structure of the Nano composite. The Fourier transform infrared spectroscopy (FTIR) spectrum of the GO/SM/Sn was also obtained through a VERTEX 70-Bruker IR spectrophotometer (Billerica, MA, USA), resolution 4 cm-1, at the wavelength range of 400–4,000 cm-1. Particle size and distribution was also measured through a Brookhaven 90Plus PALS instrument (Brookhaven Instruments Corp., Holtsville, NY, USA).

2.3 Cell Culture

SW480 and MCF-7 cell lines were obtained from Pasteur Institute, Tehran, Iran. Cells were harvested in DMEM (Dulbecco's Modified Eagle Medium) supplemented with 10 % FBS (Fetal Bovine Serum) and 1 % penicillin/streptomycin, and were incubated at 37 ℃ in a humidified environment with 5 % CO2. Cells were regularly monitored until the time they reached 80-90 % confluence.

2. 4 Cytotoxicity Assay

We performed MTT assay to determine the effect of SM and the GO/SM/Sn Nano composite on the cell viability. SW480 and MCF-7 cells were seeded in a 96-well plate, at the density of 6 × 103 cells per well, 24 h prior to treatment. After incubation, cells were treated with 0 - 500 µg/ml of SM and GO/SM/Sn for 24, 48 and 72 h. After each time span, 20 µl tetrazolium salt (5 mg/ml) was added to each well, followed by 4 h of incubation at 37℃. To dissolve formazan crystals, 200 µl DMSO was added to each well. The absorbance readings were carried out at 570 nm by the ELISA plate reader (STAT FAX 2100, USA).

2. 5 Determination of the Reactive Oxygen Species (ROS)

To determine the intracellular ROS concentration, SM and GO/SM/Sn-treated cells were dissociated and washed with PBS. After centrifugation at 1000 rpm for 5 min, 10 µl Dichloride-dihedron-fluorescein dilacerate (DCFH-DA) was added to the cell pellets and samples were incubated at 37 °C for 45 min. Cells were centrifuged and then suspended in 3 ml PBS. In the final step, fluorescent intensity was measured by the FACSCalibur flow cytometer.

2. 6 Cell Cycle Analysis

Cell population at different stages of cell cycle was determined through cell cycle assay and flow cytometers instrument. Confluent cells were treated with IC50 concentration of both SM and GO/SM/Sn for 48 h. After incubation, cells were suspended in PBS and then were fixed with cold ethanol 70 %. Next, the PI master mix solution containing 40 µl PI, 10 µl RNase and 950 µl PBS was added to each group. After 30 min of incubation at room temperature, SW480 and MCF-7 cell distribution in each stage of cell cycle was investigated through FACSCalibur flow cytometer and Flow software version 7.6.1.

2.7 Flow Cytometer and Apoptosis

To measure the apoptosis rate of both SW480 and MCF-7 cell lines after treatment with SM and GO/SM/Sn Nano composite, we used FACSCalibur flow cytometer. At first, cells were treated with IC50 concentration of SM and GO/SM/Sn for 48 h. Then trypsin zed cells were suspended in 0.5 µl Annex in-V-FLUOS, 1 ml incubation buffer and 0.5 µl presidium iodide (PI), and incubated in a dark place, at room temperature for 30 min. Finally, the apoptosis induction capacity of SM and GO/SM/Sn was analyzed through data staining and the use of Flow software version 7.6.1.

2.8 RNA isolation and real-time PCR

Total RNA was extracted from SW480 and MCF-7 cell lines, using yenta Tajhiz RNA extraction kit (Tehran, Iran). RNA purity was examined through Nano Drop 2000 spectrophotometer (Thermo Fisher Scientific, USA). Reverse transcription of the total RNA (1-5 µg) was performed according to the protocol provided by cDNA synthesis kit (Yenta Tajhiz, Tehran, Iran). Real-time PCR reactions were conducted using the ABI step one system. The reactions commenced with the initial step (5 minutes at 95 °C) and the subsequent 40 cycles of denaturation at 95 °C for 15 sec, annealing at 58-60 °C for 30 sec, and extension at 72 °C for 30 sec. Experiments were performed three times and all samples were run in duplicate. Gene expression analysis was done with the use of β-actin as the internal reference gene. Relative gene expression in each treatment group was compared with control samples and calculated based on $2^{-\Delta\Delta Ct}$ method. Table 1 highlights specific primer sequences for each gene.

Genes	Forward and Reverse Primer	Lenght	TM(°C)
BAX	F: ACCGCCTCACTCACCATCT	19	60.61
	R: GACCACTCTTCCCCACACC	19	59.62
BCL2	F: CAGACACACACACACACAACAA	22	59.77
	R: TTTACAGGCACAGAACATCCA	21	57.5
B-ACTIN	F: GGCACCCAGCACAATGAAG	19	59.41
	R: CCGATCCACACGGAGTACTT	21	59.8

Table 1. Primer sequences for *BAX, BCL2* and *β-ACTIN*.

2.9 Statistical Analysis

All data were analyzed by one-way analysis of variance (ANOaVA), with the Brown-Forsythe test and the use of Graph Pad Prism 8.0 (San Diego, USA). Obtained data were expressed as mean ± SD and data with p values lower than 0.05 were considered as statistically significant.

3. Results

3. 1 GO/SM/Sn Characterization

Figure 1A shows FT-IR spectra for (CH3)2SnCl2, SM, GO and the GO/SM/Sn Nano composite. The FT-IR spectrum of GO (Figure 1A, graph B), illustrates an intense band at 1625 cm^{-1} and 1730cm^{-1} that could be assigned to the C=C and C=O stretching vibrations of GO. In the FTIR spectrum of the SM (Figure 1A, graph C), shows that the C=O stretching vibrations of the SM at 1638 cm^{-1} shifted to 1628 cm^{-1}, so we could consider the hypothesis based on displacement of the C=O stretching vibrations of the SM to 1628 cm^{-1} (lower frequency) as a result of developing intermolecular hydrogen bonds in the GO/SM/Sn Nano composite. The FT-IR spectrum of GO/SM/Sn Nano composite (Figure 1A, graph A), shows a broad band in the region 3700 to 3000 cm-1 related to stretching vibrations of hydroxyl group OH, may be absorbed on the GO/SM/Sn nanocompsite.

Figure 1B shows XRD pattern for GO and GO/SM/Sn Nano composite. The XRD pattern of GO Nano sheet shows a relative wide peak in 2Θ = 9.1° in the complex Sn-SM this peak transferred to 2Θ = 8.4°. 2Θ decreasing indicated that inclosing in distance between GO planes in the complex, due to presence of (CH_3)2SnCl2 into the carbon layer structure.

Surface morphology, Nano composite size distribution and relative configuration of GO/SM/Sn were analyzed through FE-SEM. Elemental analysis of EDS has been highlighted in Figure 1C. This figure confirms existence of C, O, Cl and Sn elements in the structure of the synthesized GO/SM/Sn Nano composite. It was also found that weight percent of C, O, Cl and Sn in the Nano composite were 71.7, 29.5, 3.7 and 0.2, respectively. Moreover, we observed three Sn peaks in different areas of the EDS graph that showed Sn as the element in the structure of the synthesized GO/SM/Sn Nano composite.

Map elemental analysis, which has been shown in Figure 1d, shows monotonous spatial distribution of C, O, Cl and Sn elements in the nanoparticle. High density of C and O elements were revealed to be related to the SM structure, confirming the SM presence in the GO/SM/Sn Nano composite. Figure 1E illuminates that GO surface are covered by silymarin and Sn nanoparticles which could be responsible for stabilization of the Sn. TEM image has been presented in Figure 1F which shows that particles had a Nano scale and were properly distributed in the GO/SM/Sn nanocomposite that the mean diameter of the Nano composite was about 25 nm.

Distribution and the mean diameter of the synthesized Nano composite were obtained by dynamic light scattering (DLS) technique. DLS analysis (Figure 1G) showed that 1.360 RI for Sn element was indicative of 100 % particle diameter distribution in a diameter range lower than 23.4 nm. Furthermore, DLS results showed that approximately 99 % of the synthesized Nano composites had mean diameter less than 100 nm, which confirmed the TEM result.

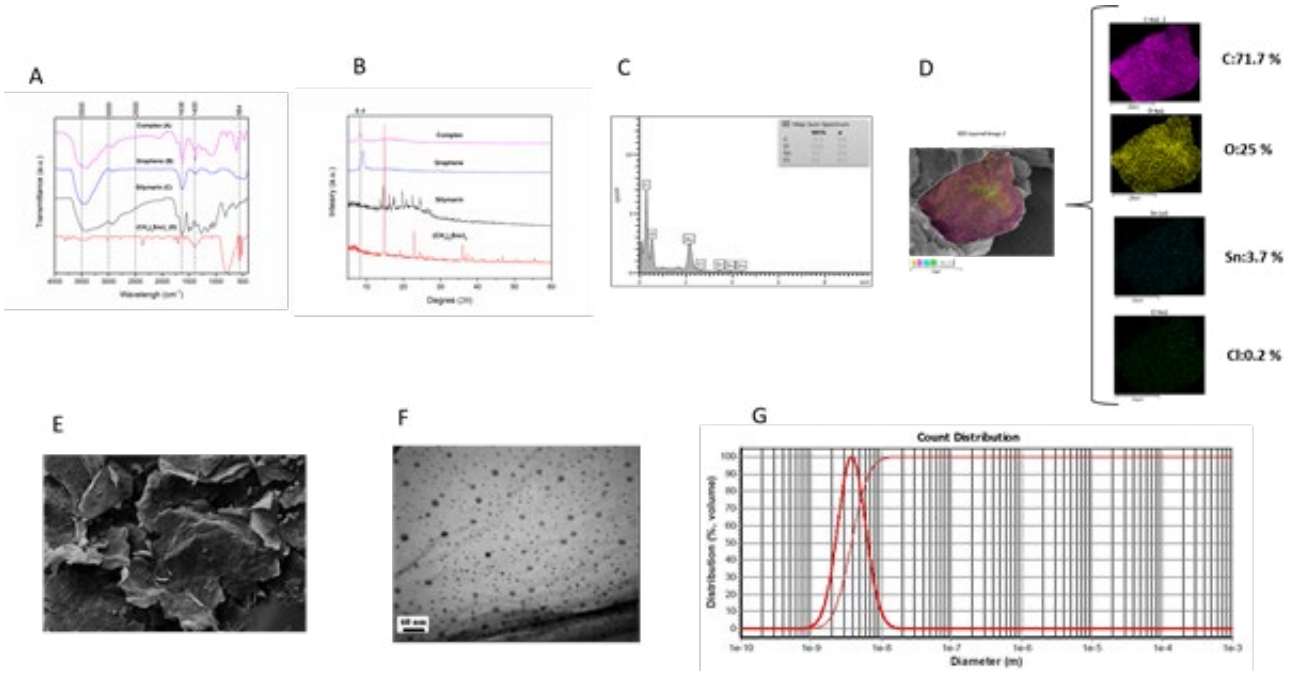

Figure 1: A. FTIR spectra of $(CH_3)_2SnCl_2$, SM, GO and GO-SM-Sn Nano composite; B. XRD patterns of $(CH_3)_2SnCl_2$, SM, GO and GO-SM-Sn Nano composite; C. EDS pattern of GO-SM-Sn Nano composite; D. Elemental mapping of the GO-SM-Sn Nano composite; E. SEM images of GO-SM-Sn Nano composite; F. TEM images of GO-SM-Sn Nano composite, G: DLS analysis and distribution of SM nanoparticles loaded on GO and Sn.

3.2 GO/SM/Sn deteriorates cancer cell viability

Cell viability under the effect of SM and GO/SM/Sn was determined using tetrazolium salt assay. Figure 2 show cell morality of SW480 and MCF-7. As it can be seen from this figure, GO/SM/Sn significantly reduced SW480 and MCF-7 cell viability in a dose dependent manner. The IC50 concentration of all treatment groups has been summarized in tables 2 for SW480 and MCF-7 cells. From these data, it can be found that the administration of GO/SM/Sn Nano composite could lessen the IC50 value of SM and elevate its ability to induce cancer cell death after 48 h.

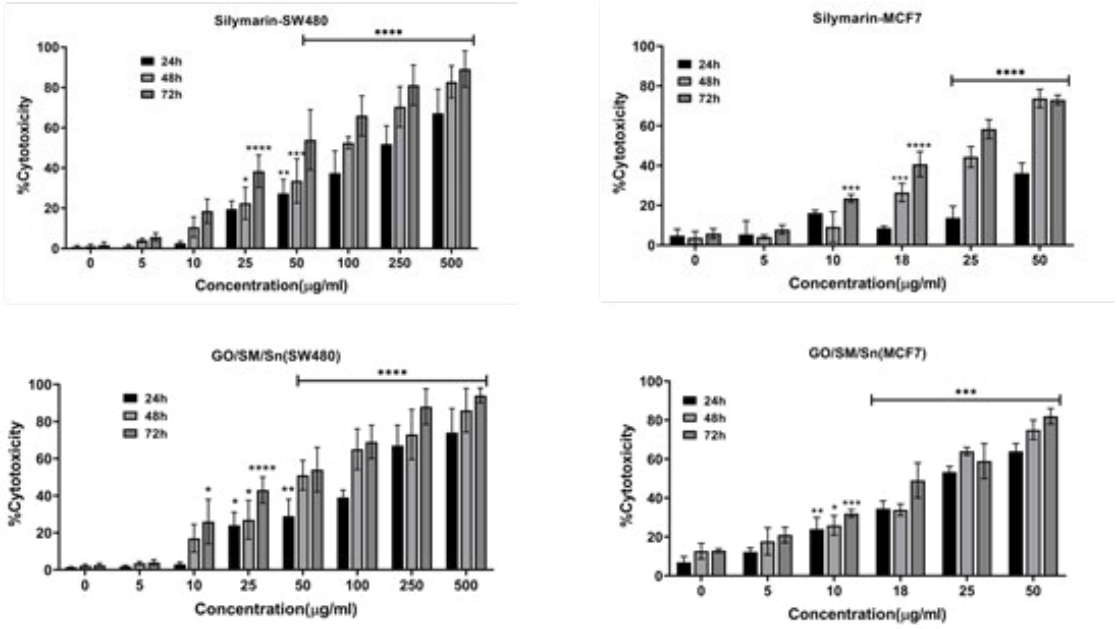

Figure 2: The cytotoxicity of SW480 and MCF7 cells after 24, 48 and 72 h treatment with various concentrations of Silymarin and GO/SM/Sn relative to untreated control; measured by MTT assay. The obtained results are presented as mean ± SD of at least three replicates (* $p < 0.05$, ** $p < 0.01$, *** $p < 0.001$, **** $p < 0.0001$ compared with the control).

treatment	24h	48h	72h
$Silymarin_{(SW480)}$	202.2	96.27	46.66
$GO/SM/Sn_{(SW480)}$	137.4	60.6	38.6
$Silymarin_{(MCF-7)}$	IC50>50	29.24	22.26
$GO/SM/Sn_{(MCF-7)}$	27.44	21.82	17.58

Table 2. Obtained IC50 value of SW480 and MCF-7 cells treatment with Silymarin and GO/SM/Sn.

3.3 GO/SM/Sn Induces Intracellular ROS Generation

In order to measure ROS production in SW480 and MCF-7 cell lines after SM and GO/SM/Sn treatment, we carried out DCFH-DA assay and the results of mean fluorescent intensity have been represented in figure 3. According to Figure 3A-C highlights the effect of SM and GO/SM/Sn on the SW480 cell ROS level. As it is appeared in this figure3G, SM treatment had no significant effect on ROS production ($p = 0.434$), while GO/SM/Sn treatment could effectively induce ROS generation in SW480 cells (*4.1 fold increase,* $p < 0.001$). Furthermore, it was revealed that ROS levels of SM-treated cells significantly differed from GO/SM/Sn-treated cells ($p < 0.01$).

Figure3D-F and 3H, ROS production in the SM-treated MCF-7 cells had a 2.5 fold increase with respect to control samples ($p < 0.05$). In addition, MCF-7 cell treatment with GO/SM/Sn led to a 3.5 fold increase in the ROS generation ($p < 0.0001$). A significant difference was also observed between intracellular ROS level of cells treated with SM and those treated with the GO/SM/Sn ($p < 0.01$).

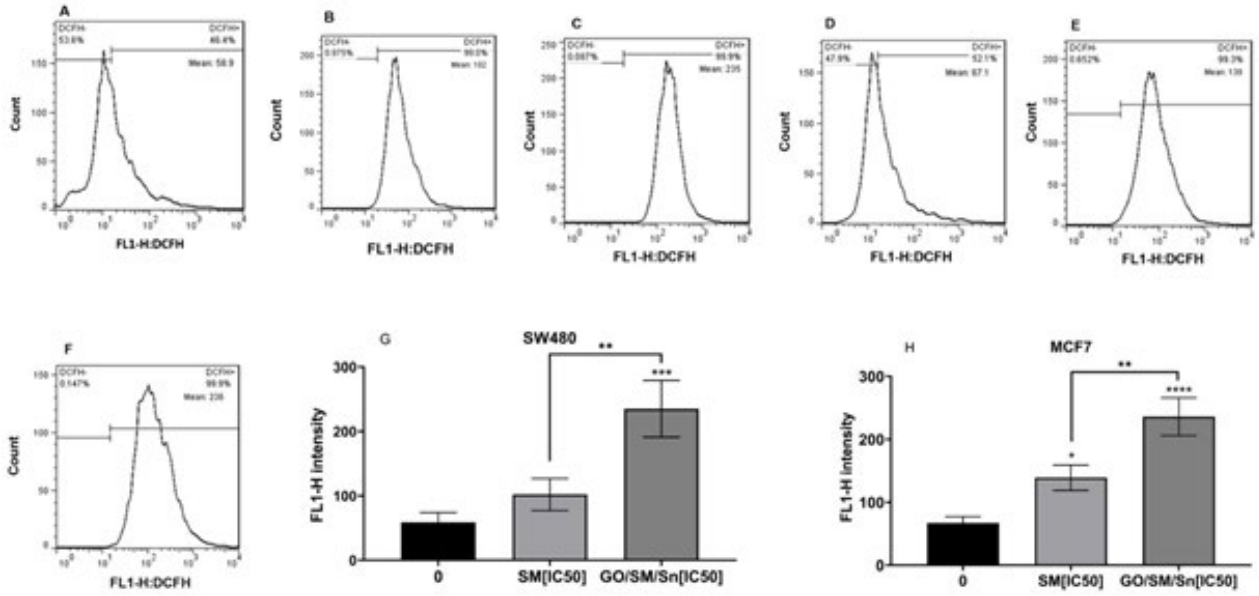

Figure 3: Mean ROS formation in the cancer cells after SM and GO/SM/Sn treatment at IC50 concentration for 48h. SW480 (A: Control; B: SM; C: GO/SM/Sn) and MCF-7 (D: Control; E: SM; F: GO/SM/Sn). The quantitative analysis was plotted to show the mean fluorescent intensity and ROS production in the SW480 (G) and MCF-7 (H) cells after treatment with SM and GO/SM/Sn nanocomposie. (* $p < 0.05$, ** $p < 0.01$).

3. 4 GO/SM/Sn modulates cancer cell cycle phases

To detect cell status at each cell cycle stage, we conducted cell cycle assay with the use of flow cytometer. The effect of SM and GO/SM/Sn on SW480 cells has been shown in figure 4A-C. Data from figure 4G show that SM and GO/SM/Sn treatment had no statistically significant effect on G0/G1 cell cycle arrest and cell population in S and G2/M phases. Cell cycle analysis in MCF-7 cells treated with SM and GO/SM/Sn Nano composite is illustrated in figure 4D-F. As figure 4H shows, SM treatment had no remarkable impact on G0/G1 phase arrest and cell population S and G2/M phases. However, GO/SM/Sn treatment was capable of inducing G0/G1 cell cycle arrest ($p \leq 0.05$) and decreasing cell population in S cell cycle phase ($p \leq 0.05$). Moreover, GO/SM/Sn treatment had also no significant effect on cell population in G2/M phase. Table 3 summarizes quantitative changes in the cell cycle phases of SW480 and MCF-7 cell lines.

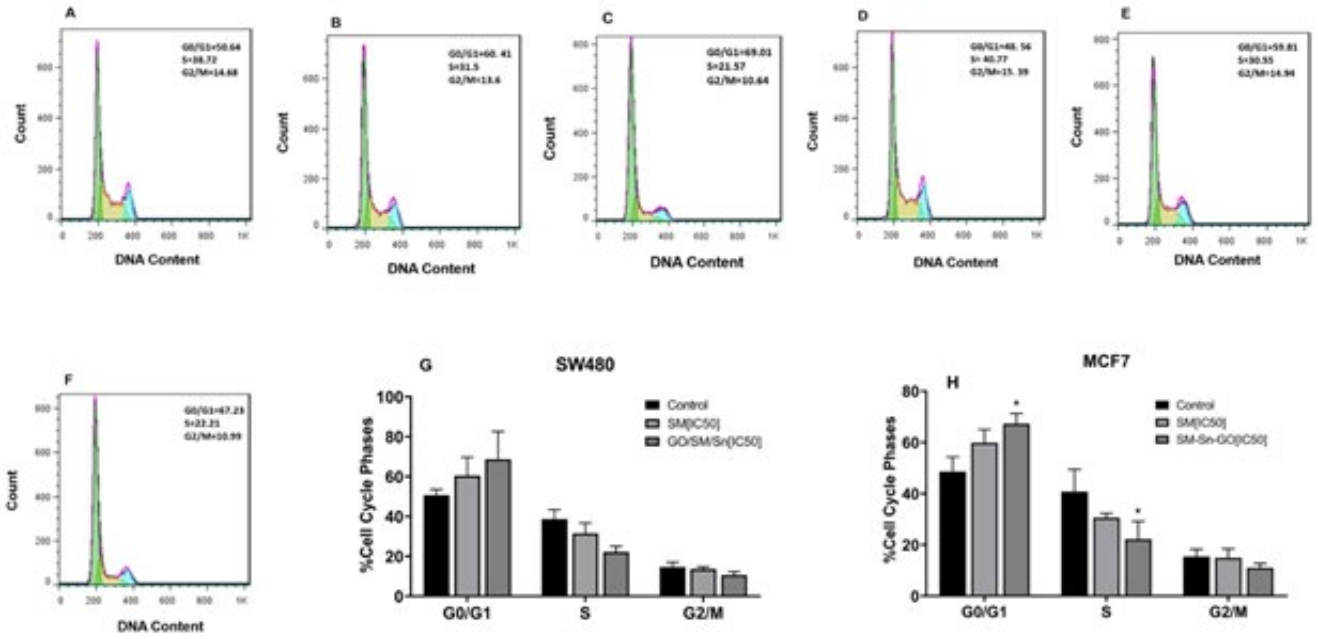

Figure 4: Cell cycle phases in the cancer cells after SM and GO/SM/Sn treatment at IC50 concentrations for 48h. SW480 (A: Control; B: SM; C: GO/SM/Sn) and MCF-7 (D: Control; E: SM; F: GO/SM/Sn). Quantitative comparison of cell cycle arrest in SW480 (G) and MCF-7 (H) cells after SM and GO/SM/Sn treatment (* $p < 0.05$ compared with the control).

Group	G0/G1 Phase	S Phase	G2/M Phase
SW480			
Control	50.64±2.887	38.72 ± 4.619	14.68 ± 2.309
SM	60.41±9.23) p=0.523)	31.5 ±5.196 (p=0.698)	13.6 ± 1.55 (p=0.99)
GO/SM/Sn	69.51±13.85 (p=0.129)	21.57 ± 2.84 (p=0.177)	10.46 ± 1.723 (p=0.89)
MCF7			
Control	48.56 ± 5.77	40.77 ± 8.6	15.39 ± 2.88
SM	59.81 ± 5.196 (p=0.27)	30.55 ± 1.73 (p=0.34)	14.94 ± 3.4 (p=0.99)
GO/SM/Sn	67.23 ± 4.04 (p≤0.05)	22.1 ± 6.92 (p≤0.05)	10.99 ± 1.73 (p=0.81)

Table 3: Quantitative comparison of cell cycle arrest, 48 h after SW480 and MCF-7 cell treatment with SM and GO/SM/Sn on IC50 concentration at 48h.

3.5 GO/Sn/Sn Increases Cancer Cell Apoptosis Rate

Quantification of apoptosis for both SW480 and MCF-7 cell lines was performed by Annexing V binding, PI uptake and flow cytometer. SW480 cells treated with GO/SM/Sn exhibited lower cell viability ($p < 0.001$) and higher apoptosis rate after 48 h ($p < 0.01$). This effect was significant as compared to SM-treated SW480 cells and control group (figure 5A-C and 5G). Furthermore, the effect of SM and GO/SM/Sn on the MCF-7 cell apoptosis rate is presented in figure 5D-E and 5H. These figures indicate that in comparison with SM-treated and control samples, GO/SM/Sn treatment remarkably reduced cell viability ($p < 0.0001$) and induced apoptosis ($p < 0.0001$). Table 3 shows detailed data regarding the impact of SM and GO/SM/Sn treatment on the live and apoptotic cells. Interestingly, we observed increased necrotic cell population after GO/SM/Sn treatment, however, this data was not statistically significant for both cell lines.

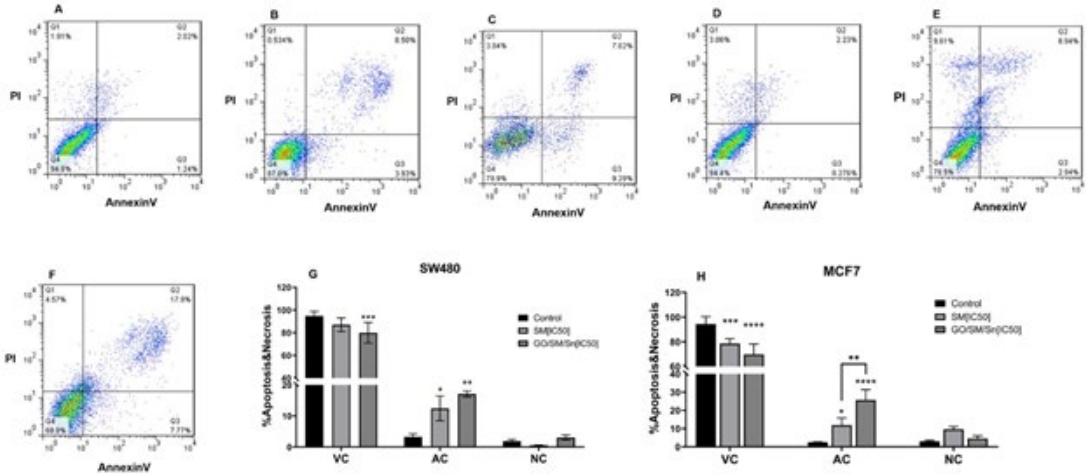

Figure 5: SW480 and MCF7 cell percent in different phases of Annexing/PI after treatment with SM and GO/SM/Sn at IC50 concentration for 48h; SW480 (A: Control; B: SM; C: GO/SM/Sn) and MCF-7 (D: Control; E: SM; F: GO/SM/Sn). Q1 indicates necrotic cells with An^-/PI^+; Q2 is related to late apoptotic cells with An^+/PI^+; Q3 shows early apoptotic cells with An^+/PI^-; and Q4 represents live cells with An-/PI-.Quantitative comparison of apoptosis after SW480 (G) and MCF7 (H).Abbreviation: VC, viable cells; AC, apoptotic cells; NC, necrosis cells.

Group	Viable Cells	Apoptotic Cells	NecroticCells
SW480			
Control	94.8 ± 2.3	3.26 ± 0.577	1.91 ± 0.289
SM	87.0 ± 3.46 (p=0.07)	12.43 ± 2.309 (p<0.05)	0.534 ± 0.058 (p=0.91)
GO/SM/Sn	79.9 ± 5.259 (p<0.001)	17.11 ±0.572 (p<0.01)	3.04 ± 0.462 (p=0.94)
MCF7			
Control	94.4±3.4	2.506 ± 0.102	3.06 ± 0.289
Silymarin	78.5 ± 2.903 (p<0.001)	11.88 ± 2.252(p<0.05)	9.61 ±0.866(p=0.92)
GO/SM/Sn	69.8 ± 4.85(p<0.0001)	25.67 ± 3.291(p<0.0001)	4.57 ± 0.866 (p=0.94)

Table 4. Quantitative comparison of apoptosis, necrosis and live cells, 48 h after SW480 and MCF-7 cell treatment with SM and GO/SM/Sn on IC50 concentration at 48h.

3.6 GO/SM/Sn Stimulates Apoptotic Gene Expression

BAX and *BCL2* gene expression were analyzed using specific primer sequences and real-time PCR system. Figure 6A shows the effect of SM and GO/SM/Sn treatment on *BAX* and *BCL2* gene expression in SW480 cells. As compared with SM-treated and control samples, GO/SM/Sn significantly up regulated *BAX* gene expression ($p \leq 0.05$), while did not remarkably impact *BCL2* gene expression. *BAX* and *BCL2* gene expression analysis in MCF-7 cells (figure 6B) showed that GO/SM/Sn treatment led to the increased *BAX* expression ($p < 0.0001$) and reduced *BCL2* mRNA levels ($p \leq 0.05$). In addition, the *BAX/BCL2* ratio was found to be higher than 1 in SW480 and MCF-7 cells treated with GO/SM/Sn.

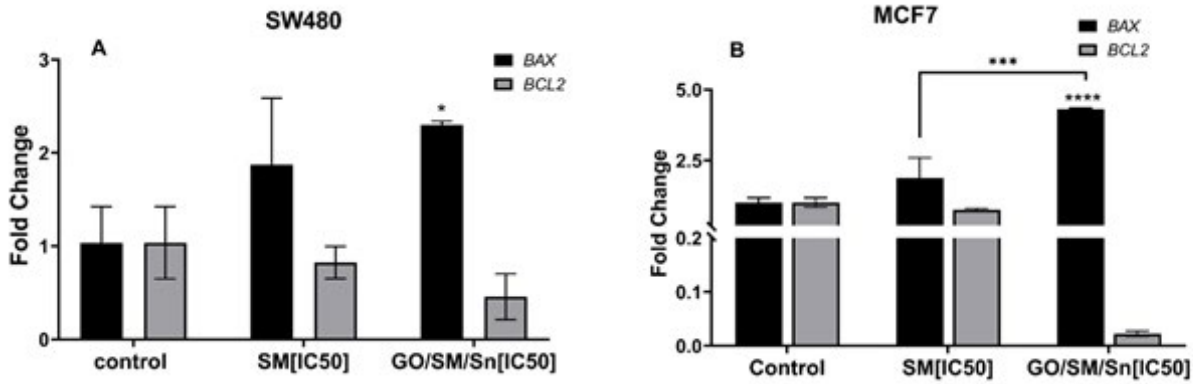

Figure 6: BAX and BCL2 gene expression and in SW480 (A) and MCF7 (B) cells, 48 h after SM and GO/SM/Sn treatment a IC50 concentration. (* p < 0.05, ** p < 0.01, *** p < 0.001, **** p < 0.0001 compare with the control).

4. Discussion

Cancer begins as the result of several genetic derangements, leading to cell growth and division in an uncontrolled manner. Cancerous cells proliferate faster than normal cells and this property help them to form tumors in body tissues. In spite of emerging advanced treatment strategies, there is still a great deal of challenge with cancerous cells and tissues due to development of drug resistance as the consequence of genetic mutations, epigenetic changes and other cellular and molecular events. Therefore, designing novel treatment approaches without any serious side effects is of paramount importance. For this particular purpose, we introduced a Nano formulation of SM loaded on $(CH_3)_2SnCl_2$ based on GO to achieve enhanced cytotoxicity at very low dose in SW480 and MCF-7 cell lines [15, 16].

Herein, we attempted to synthesize a GO-based $(CH_3)_2SnCl_2$ scaffold to increase the solubility and bioavailability of SM. The ant proliferative and antitumor activity of Sn have been reported in previous studies. Interestingly, grapheme oxide has been considered as a non-invasive option to increase the efficiency of anticancer drug delivery. Shape and size of the introduced Nano composite or microstructure are the most important properties during *in vitro* investigations of cytotoxicity. From the aforementioned data it is clear that the synthesized Nano composite had an extended surface and a Nano scale. These properties led the Nano composite to effectively contribute to cancer cell death. More precisely, our results of cytotoxicity analysis indicated that GO/SM/Sn has lower IC50 value than that of SM in the tested cancer cell lines. This finding further supports the idea of Snima et al, who reported that silymarin-PLGA Nano composites have aIC50 value lower than that of silymarin. The IC50 is considered as a criteria for inhibitory strength of drugs and agents, that is, lower IC50 means higher inhibitory effect [17-24].

One of our important findings was decreased cell viability and increased apoptosis rate under the effect of GO/SM/Sn Nano composite. This finding is consistent with the study of Upadhyay *et al,* which demonstrated that HepG2 cell treatment with Nano encapsulated silymarin inhibits cell proliferation and induces apoptosis. We also found that GO/SM/Sn treatment was capable of inducing *BAX* and reducing *BCL2* gene expression in both SW480 and MCF-7 cell lines. It is interesting to compare these effects with that of silibinin, a major component of SM. These findings accord with previous observations, which showed that silibinin and Nano formulated SM are potent inducers of *BAX* expression and inhibitors of the *BCL2* gene levels [25-29].

The current study found that cell treatment with GO/SM/Sn is capable of inducing intracellular ROS production in both SW480 and MCF-7 cell lines. This result is in agreement with a very recent study, which showed that SM Nano emulsion leads to surged ROS levels and the ensuing hepatic cancer cell death. These findings suggest that SM Nano-encapsulation is capable of improving its oral administration and bioavailability [30].

Another important finding of this study was increased cell cycle arrest under the effect of GO/SM/Sn treatment. However, this effect revealed to be statistically insignificant. Interestingly, MCF-7 cell treatment with GO/SM/Sn could remarkably arrest cell cycle. These results are in line with those of others and suggest a promising role of SM immobilization in the induction of cancer cell death [25, 26].

5. Conclusion

Returning to the hypothesis posed at the beginning of this study, it is now possible to state that GO/SM/Sn formulation is probably a novel option for diminishing adverse side effects of the conventional treatment approaches. The most obvious finding to emerge from this study is that the introduced GO/SM/Sn formulation can remarkably hinder cancer cell growth and proliferation. Taken together, the results of this study can pave the way toward understanding detailed curative effects of GO/SM/Sn Nan composite in the future. More importantly, further work needs to be done to establish the impact of GO/SM/Sn formulation on cell surface receptors and gene expression profile of cancer cells.

Acknowledgement

The authors thank Shabnam Bandad in the Pharmaceutical Sciences Center, Tehran Medical Sciences, Islamic Azad University and Tehran, Iran for her technical collaborations.

Funding: This research did not receive any specific grant from funding agencies in the public, commercial, or not-for-profit sectors.

Ethics statement

The current study was approved by the ethics committee number of IR.IAU.PS.REC.1400.085, Tehran Medical Sciences, Islamic Azad University, Tehran, Iran.

Declaration of competing interest

All authors declare that they have no personal or financial competing interest that could have impacted this research work.

References

1. Bray, F., Farley, J., Soerjomataram, I., Siegel, R. L., Torre, L. A., & Jamal, A. (2018). GLOBOCAN estimates of incidence and mortality worldwide for 36 cancers in 185 countries: Global cancer statistics. CA Cancer J Cline, 68(6), 394-424.
2. Boyle, P., & Levin, B. (2008). World cancer report 2008. IARC Press, International Agency for Research on Cancer.
3. Khan, H., Gullah, H., Marmoreal, M., Valdes, S. E., Belwal, T., Tejada, S., & Kamal, M. A. (2021, February). Flavonoids nanoparticles in cancer: Treatment, prevention and clinical prospects. In Seminars in cancer biology (Vol. 69, pp. 200-211). Academic Press.
4. Fu, B., Wang, N., Tan, H. Y., Li, S., Cheung, F., & Feng, Y. (2018). Multi-component herbal products in the prevention and treatment of chemotherapy-associated toxicity and side effects: a review on experimental and clinical evidences. Frontiers in Pharmacology, 9, 1394.
5. Hayat, M. J., Holder, N., Reich man, M. E., & Edwards, B. K. (2007). Cancer statistics, trends, and multiple primary cancer analyses from the Surveillance, Epidemiology, and End Results (SEER) Program. The oncologist, 12(1), 20-37.
6. Liu, Y. Q., Wang, X. L., He, D. H., & Cheng, Y. X. (2021). Protection against chemotherapy-and radiotherapy-induced side effects: A review based on the mechanisms and

therapeutic opportunities of phytochemicals. Phytomedicine, 80, 153402.
7. Craggy, G. M., & Pezzuto, J. M. (2016). Natural products as a vital source for the discovery of cancer chemotherapeutic and chemo preventive agents. Medical Principles and Practice, 25(Suppl. 2), 41-59.
8. N Nwodo, J., Ibezim, A., Simoben, C. V., & Ntie-Kang, F. (2016). Exploring cancer therapeutics with natural products from African medicinal plants, part II: alkaloids, terpenoids and flavonoids. Anti-Cancer Agents in Medicinal Chemistry (Formerly Current Medicinal Chemistry-Anti-Cancer Agents), 16(1), 108-127.
9. Madrigal-Santillán, E., Madrigal-Bujaidar, E., Álvarez-González, I., Sumaya-Martínez, M. T., Gutiérrez-Salinas, J., Bautista, M., & Morales-González, J. A. (2014). Review of natural products with hepatoprotective effects. World journal of gastroenterology: WJG, 20(40), 14787.
10. Delmas, D. (2020). Silymarin and derivatives: From biosynthesis to health benefits. Molecules, 25(10), 2415.
11. Won, D. H., Kim, L. H., Jang, B., Yang, I. H., Kwon, H. J., Jin, B.,... & Cho, S. D. (2018). In vitro and in vivo anti-cancer activity of silymarin on oral cancer. Tumor Biology, 40(5), 1010428318776170.
12. Yang, K. Y., Hwang, D. H., Yousef, A. M., Kim, D. W., Shin, Y. J., Bee, O. N.,... & Choi, H. G. (2013). Silymarin-loaded solid nanoparticles provide excellent hepatic protection: physicochemical characterization and in vivo evaluation. International journal of Nan medicine, 3333-3343.
13. Congas, M., Kutlu, H. M., Burukoglu, D. D., & Ayhancı, A. (2015). A comparative study on the therapeutic effects of silymarin and silymarin-loaded solid lipid nanoparticles on D-GaIN/TNF-α-induced liver damage in Balb/c mice. Food and Chemical Toxicology, 77, 93-100.
14. Abbasi, F., Samadi, F., Jafari, S. M., Ramezanpour, S., & Shargh, M. S. (2019). Ultrasound-assisted preparation of flaxseed oil Nano emulsions coated with alginate-whey protein for targeted delivery of omega-3 fatty acids into the lower sections of gastrointestinal tract to enrich broiler meat. Ultrasonic Son chemistry, 50, 208-217.
15. Shukla, K. K., Tiwari, A., & Sharma, S. (2017). Classification of histopathological images of breast cancerous and non-cancerous cells based on morphological features. Biomedical and Pharmacology Journal, 10(1), 353-366.
16. Wang, X., Zhang, H., & Chen, X. (2019). Drug resistance and combating drug resistance in cancer. Cancer Drug Resistance, 2(2), 141.
17. Rocamora-Reverte, L., Carrasco-Garcia, E., Ceballos-Torres, J., Prather, S., Kaluđerović, G. N., Farragut, J. A., & Gómez-Ruiz, S. (2012). Study of the anticancer properties of tin (IV) carboxylate complexes on a panel of human tumor cell lines. ChemMedChem, 7(2), 301-310.
18. Ismael, S. A. A., Shames, M., Chen, T., & Al-abbacy, W. M. (2019). Design, synthesis and characterization of tin-based cancer chemotherapy drug entity: In vitro DNA binding, cleavage, induction of cancer cell apoptosis by triggering DNA damage-mediated p53 phosphorylation and molecular docking. Applied Organometallic Chemistry, 33(1), e4651.
19. Chung, C., Kim, Y. K., Shin, D., Ryoo, S. R., Hong, B. H., & Min, D. H. (2013). Biomedical applications of grapheme and grapheme oxide. Accounts of chemical research, 46(10), 2211-2224.
20. Jung, H. S., Kong, W. H., Sung, D. K., Lee, M. Y., Beak, S. E., Krum, D. H.,... & Hahn, S. K. (2014). Nanographene oxide–hyaluronic acid conjugate for photo thermal ablation therapy of skin cancer. ACS Nano, 8(1), 260-268.
21. Li, Y., GAO, W., Chi, L., Wang, C., & Aja an, P. M. (2010). Catalytic performance of Pt. nanoparticles on reduced grapheme oxide for methanol electro-oxidation. Carbon, 48(4), 1124-1130.
22. Yang, Y., Azeri, A. M., Tang, Z., Du, D., & Lin, Y. (2013). Graphene based materials for biomedical applications. Materials today, 16(10), 365-373.
23. Snima, K. S., Arunkumar, P., Jayakumar, R., & Lakshmanan, V. K. (2014). Silymarin encapsulated poly (D, L-lactic-co-glycolic acid) nanoparticles: a prospective candidate for prostate cancer therapy. Journal of biomedical nanotechnology, 10(4), 559-570.
24. Ghiberti, G., Brochette, G., & Luciana, L. (2020). Interactions between phenolic compounds, amyl lytic enzymes and starch: An updated overview. Current Opinion in Food Science, 31, 102-113.
25. Upadhyay, P., Bhattacharjee, M., Bhattacharya, S., Ahir, M., Adhikary, A., & Patra, P. (2020). Silymarin-loaded, lactobionic acid-conjugated porous PLGA nanoparticles induce apoptosis in liver cancer cells. ACS Applied Bio Materials, 3(10), 7178-7192.
26. El-Far, M., Salah, N., Essam, A., Abd El-Azim, A. O., & El-Sherbiny, I. M. (2018). Silymarin nanoformulation as potential anticancer agent in experimental Ehrlich ascites carcinoma-bearing animals. Nanomedicine, 13(15), 1865-1858.
27. Kim, S. H., Choo, G. S., Yoo, E. S., Woo, J. S., Han, S. H., Lee, J. H., & Jung, J. Y. (2019). Silymarin induces inhibition of growth and apoptosis through modulation of the MAPK signaling pathway in AGS human gastric cancer cells. Oncology reports, 42(5), 1904-1914.
28. Jahanafrooz, Z., Mortimer, N., & Bakhshandeh, B. (2016). Comparative evaluation of silibinin effects on cell cycling and apoptosis in human breast cancer MCF-7 and T47D cell lines. Asian Pacific Journal of Cancer Prevention, 17(5), 2661-2665.
29. Zhang, M., Liu, Y., Go, Y., & Li, S. (2015). Silibinin-induced glioma cell apoptosis by PI3K-mediated but Act-independent down regulation of FoxM1 expression. European journal of pharmacology, 765, 346-354.
30. Ahmad, U., Akhtar, J., Singh, S. P., Bedridden, Ahmad, F. J., Siddiqui, S., & Wahajuddin. (2018). Silymarin Nano emulsion against human hepatocellular carcinoma: development and optimization. Artificial cells, Nano medicine, and biotechnology, 46(2), 231-241.